

**ROYAL SOCIETY
OPEN SCIENCE**

R. Soc. open sci.

doi:10.1098/ not yet assigned

**This is a preprint, and may be subject to further revisions.
Please note that subsequent versions may have different
content.**

Volcanic hazard exacerbated by future global warming-driven increase in heavy rainfall

Jamie I. Farquharson,^{1,†} Falk Amelung¹

¹Rosenstiel School of Marine and Atmospheric Science, University of Miami, Miami, FL, USA

Keywords: Climate change; Volcanism; General circulation model; Precipitation; Geosphere–Hydrosphere interaction; Climate forcing

1. Summary

Heavy rainfall drives a range of eruptive and noneruptive volcanic hazards; over the Holocene, the incidence of many such hazards has increased due to rapid climate change. Here we show that extreme heavy rainfall is projected to increase with continued global warming throughout the 21st century in most subaerial volcanic regions, increasing the potential for rainfall-induced volcanic hazards. This result is based on a comparative analysis of nine general circulation models, and is prevalent across a wide range of spatial scales, from countries and volcanic arcs down to individual volcanic systems. Our results suggest that if global warming continues unchecked, the incidence of primary and secondary rainfall-related volcanic activity—such as dome explosions or flank collapse—will increase at more than 700 volcanoes around the globe. Improved coupling between scientific observations—in particular, of local and regional precipitation—and policy decisions may go some way towards mitigating the increased risk throughout the next 80 years.

2. Climate change and volcanism

The role of Earth's subaerial volcanism in driving past climate changes has been substantial [1]—due in large part to the radiative and chemical effects of erupted gases and aerosols [2]—and it is anticipated to drive further variability in the future [3,4]. In turn, variations in climate have also been posited to drive volcanic activity [5–9]. Mechanisms such as the isostatic unloading of the crust due to warming-induced glacial retreat and ice cap melt [10,11] or crustal stress changes generated by changing sea levels [12] have been proposed to promote volcanic activity over a range of spatio-temporal scales. Over the last 30 ka, changes in climate have driven an increase in massive volcanic collapses, partly in response to increased humidity and rainfall [13]. An uptick in rainfall-driven volcanic hazards has been proposed for many volcanic regions as global climate continues to warm throughout the Anthropocene; in particular, in unglaciated high-relief volcanic environments [7]: an observable rate change in hazardous geological phenomena that may already be underway [14].

Extreme or seasonal rainfall has been identified as a trigger mechanism for primary volcanic activity—discrete eruptions of lava, tephra, and gases—at multiple volcanoes. Examples include rainfall-triggered explosions at Mount St Helens (USA), Gunung Merapi (Indonesia), and Las Pilas (Nicaragua) [15–17]. Coupling between extreme rainfall events and dome collapse has also frequently been noted [18–22], with heavy rainfall also being linked to the generation of pyroclastic density currents [21]. More recently, a link between extreme rainfall, pore fluid changes at depth, and magma propagation has been proposed at Kīlauea Volcano, USA [23] and Etna, Italy [24]. Rainfall-triggered volcanism is often violently explosive [15], and multiple direct fatalities have been recorded as a result, including at Karkar [25], Guagua Pichincha [26], and Karangetang [27] volcanoes (Papua New Guinea, Ecuador, and Indonesia, respectively). Many hazards associated with extreme precipitation events or prolonged rainfall are heightened in volcanic regions: not only do mountainous regions tend to modify and amplify precipitation [28], but they are often mantled by variably consolidated tephra deposits and other easily mobilised debris, and can be associated with large thermal gradients. These gradients drive explosive fuel-coolant interactions [29], and thermal atmospheric forcing due to volcanic thermal anomalies can also increase precipitation above the threshold required to trigger hazards [30]. These factors promote a range of rainfall-related secondary volcanic hazards, including the remobilisation of volcanogenic deposits in the form of lahars [31–33] and the instigation of flank mass movement [34–37], a phenomenon that can in turn unload the magma chamber and promote explosive decompression or dyke initiation [38]. Volcanic slopes, typically with low cohesion and narrow grain-size distributions, may be particularly disposed to mass wasting events [37].

*Author for correspondence (jifarq89@googlemail.com).

†Present address: Université de Strasbourg, France

The timing, distribution, and amount of rainfall received by active volcanic systems is influential over a range of timescales. **Figure 1a** indicates catastrophic Pleistocene sector collapses of four volcanoes in Mexico: Volcán de Colima, Nevado de Toluca, Citlaltépetl, and Cofre de Perote. In all cases, depositional sequences show evidence of water saturation, hydrothermal alteration, and/or water circulation within the pre- and syn-collapse edifice. In light of the lack of systematic concomitant magmatic activity, pluvial conditions have instead been proposed to have triggered these volcanic collapses [39]. Tellingly, each of the events are associated with timeframes characterised by locally high precipitation, typically concurrent with elevated global temperatures. Similar climatic forcing of volcanic collapse has been identified for volcanoes in Europe [40] and South America [41]. Links also exist over shorter timescales: at Lokon-Empung, a triggered volcanic eruption (22 February 2011) coincided with the quarterly rainfall maximum (**Fig. 1b, c**). **Figure 1d** illustrates the intimate correlation between elevated rainfall and lahar generation (i.e., the propagation of potentially devastating pyroclastic slurries) at Mt Pinatubo (Philippines), with a lag of less than one day (**Fig. 1e**). Finally, **Fig. 1f** shows the hours-to-minutes lahar response (reflected in Real-time Seismic-Amplitude Measurement: RSAM) at Merapi. For both Pinatubo and Merapi, cross-correlation analysis reveals that lahar occurrence is related to heavy rainfall with a sub-daily lag (as low as ten minutes in the case of the latter: see **Fig. 1e, g**). Although **Fig. 1** highlights just a handful of volcanoes, a textual analysis of the Smithsonian's Global Volcanism Program Bulletin Reports—a multidecadal catalogue of reports of volcanic activity—reveals that extreme or heavy rainfall has been implicated in triggering or exacerbating hazards at at least 174 discrete volcanoes: around 13 %, or 1 in every 7 of Earth's subaerial volcanic inventory (see **Methods**).

As the rate of global climate change continues to accelerate, it becomes ever more crucial to develop a comprehensive understanding of the manifold interactions and feedbacks between the atmosphere, cryosphere, and solid Earth: complexly interconnected components of the Earth system. Here we focus on the role of heavy rainfall in volcanic environments, and the evolution of rainfall rates over a multi-decadal timeframe induced by the ongoing rapid changes in global climate. A key problem with identifying volcanic regions at increasing risk has been the inherent uncertainty of climate modelling [7]. While there is broad consensus as to the direction of mean global precipitation change [42,43], global climate models (general circulation models: GCMs)—even when initiated with the same parameters—do not show general concurrence upon the magnitude or spatial distribution of precipitation change, and observations of global mean precipitation changes are at often odds with projected changes [44]. Consistently, however, these models project an increase in the intensity and frequency of heavy precipitation—that is, extreme precipitation events—both on global and regional scales [45]. Fischer et al. [46] and Pfahl et al. [47] demonstrate that global climate models tend to concur when considering future heavy precipitation. In particular, those authors found that most models tested in their analysis agreed on the sign of change of the diurnal maximum precipitation over time at any given location.

In this contribution, we analyse a suite of numerical global climate models to assess which of Earth's subaerial volcanoes are projected to experience increases or decreases in extreme rainfall, revealing several volcanic systems which we estimate will become more susceptible to rainfall-induced hazards over the next 80 years. In particular we focus on the forced model response (FMR), the percentage change of heavy precipitation for a given unit of global warming, which serves as a proxy for the likelihood of extreme rainfall events, calculated from nine Coupled Model Intercomparison Project Phase 5 (CMIP5) general circulation models (**Methods**).

3. Materials and Methods

a. Climate proxy and volcanic hazard data

Figure 1a is reproduced after [39], using magnetic susceptibility data from lake sediment core from Pete-Itzá, Guatemala [48] (interpreted to reflect changes in summer precipitation), speleothem calcite $\delta^{18}\text{O}$ data from central New Mexico [49] (interpreted to reflect changes in winter precipitation), and the Greenland Ice Sheet Project 2 $\delta^{18}\text{O}$ [50] as a proxy for global temperature. Precipitation data in **Figure 1b** from Stasiun Geofisika Winangun (lon, lat: 124.83890, 1.44340) were accessed from Indonesia's Meteorology, Climatology and Geophysics Agency (Badan Meteorologi, Klimatologi, dan Geofisika: BMKG) data retrieval portal (<https://www.bmkg.go.id/>). Daily data of **Figure 1d** are from [51]. Merapi rainfall and RSAM data (**Figure 1f**) were digitised from [52].

b. Textual analysis of Bulletin Reports

Geolocation data for Earth's subaerial volcanoes are obtained from the Smithsonian's Global Volcanism Program (GVP) databases [53] using the GVP webservice interface. We concentrate on volcanic systems active in the Holocene (discounting volcanoes defined as primarily submarine or subglacial): 1234 volcanoes. The prior association of any particular volcano with rainfall-related volcanic hazard was determined by programmatically querying the catalogue GVP Bulletin Reports for the (case-insensitive) string literals "lahar," "heavy rain," "rainfall-triggered," "rainfall-induced," and "extreme rainfall" (ignoring punctuation and capitalisation). The crawled reports were then manually parsed to identify volcanoes with previous evidence for volcanic hazard caused or exacerbated by rainfall, and to remove reports where rainfall was mentioned in non-hazard contexts (for example, reports on the effect of rainfall on monitoring equipment or the volcanic system that do not constitute a clear hazard, geographical background descriptions, or observational and logistical difficulties associated with inclement weather). The remaining catalogue refers

specifically to hazards associated with heightened rainfall activity: steam explosions; the instigation of lahars and mudflows; column collapse and pyroclastic density current generation; landslides, rockfalls, and other mass wasting events; flooding due to crater lake overflow; and triggered primary volcanic activity.

c. Forced model response

Ensemble climate projection experiment data were obtained from the Coupled Model Intercomparison Project Phase 5 (CMIP5). CMIP5 comprises a set of coordinated climate model experiments, performed by several independent modelling groups using more than 50 discrete Earth System models, with the goal of providing a multi-model assessment of simulated climate change (and variability thereof) over timescales from decades to centuries. For a more comprehensive background to CMIP5, the reader is referred to [54]. Here, we use data from nine separate models (an “ensemble of opportunity” [55]), listed in **Supplementary Information Table S1**, each of which follow the Representative Concentration Pathway (RCP) 8.5 scenario (a “high emissions” scenario). The total period covered by the selected data is from 2005 or 2006 to 2100. For comparability, we use models from ensemble r1i1p1 only (i.e., the initial conditions and the constitutive model physics are the same, and differences in simulations reflect internal inter-model variability), at a monthly frequency. For each model and each year over the modelled period, we calculate the mean global temperature $\langle T \rangle$ timeseries and the maximum monthly rainfall value RXm for each grid cell. The forced model response (FMR) is calculated as the slope of a linear regression of RXm versus $\langle T \rangle$ normalised to 01-Jan-2006 (**Fig. 2, Supplementary Information Figure S1**) or 01-Jan-2021 (**Fig. 3 and Fig. 4**). The resulting 2D array A_k , where k is the number of the model, has dimensions dependent on the initial spatial resolution of the model experiments (**Supplementary Information Table S1**). For each model k , the value of each cell at latitude i and longitude j is binarised such that $B_{ijk} = H(A_{ijk})$ where $H(x)$ is the Heaviside function and the boolean units 0 and 1 thus denote negative and positive forced model responses, respectively. To determine areas where the majority of models agree on the sign of heavy precipitation change, we resample the binary arrays onto a common 180×360 grid (i.e., $\sim 1 \times 1^\circ$) using a nearest-neighbour approach, then sum them such that $C = \sum_{k=1}^N B_k$. Agreement in the sign of normalised RXm across at least seven of nine models is represented by $|C_{ij} - (9/2)| > 2$, where $C_{ij} \in [0,9]$. This criterion (7/9 models or 78 % model agreement) is comparable to the threshold imposed by previous studies [46,47]. Calculated forced model responses from the individual CMIP5 general circulation models are shown in **Supplementary Information Figure S1**.

d. Distribution statistics and other calculations

Additional analyses were performed on an *ad hoc* basis for individual systems or sets; for completeness, these methods are described here. Where appropriate, maxima and mean volcano flank slope values were calculated using the database compiled by [56]. Uniformity was tested for using the chi-squared (χ^2) method. Statistical significance was ascribed where the cumulative distribution function of the chi-squared statistic $CDF(\chi^2)$ was less than 0.01. Descriptive statistics of volcano FMR distributions (**Fig. 2c**) were calculated assuming a normal distribution (“negative” and “ambiguous”) and a log-normal distribution (“positive”). Cross-correlation analysis of Pinatubo and Merapi lahar data was performed by treating rainfall and lahar data as 1-dimensional sequences. **Figure 1e and 1g** show the correlation coefficient for each lag value, in days (Pinatubo) or minutes (Merapi). Correlation maxima are 0 days and 10 minutes, respectively, indicating a relatively short lag between heavy rainfall and lahar occurrence at both sites. All analyses were performed in Python.

4. Results and Discussion

a. Climate models agree on the direction of heavy precipitation change with global warming

Calculated forced model responses from the individual CMIP5 general circulation models are shown in **Supplementary Information Figure S1**, presented in % C as the gradient of a regression between monthly heavy precipitation change RXm and global mean temperature $\langle T \rangle$. There is qualitative agreement in many areas across models: less extreme rainfall is forecast by most models for the majority of Australia, parts of Saharan and southern Africa, and Central America, for example, whereas large portions of North America, Eurasia, East Africa, and the Polar regions are projected to experience an increase in extreme precipitation with continued global warming. This is emphasised by mean response of all models resized onto a common grid (**Fig. 2a**). The areas where fewer than seven of nine models agree on the sign of FMR are shaded. The area over which at least seven of nine models concur accounts for 73.45 % of the globe, in line with previous multi-model studies [46,47], despite the fact that the cited studies examine models at a daily resolution over longer timescales (including historical simulations) and analyse more models (15 and 22, respectively). As well as the proportion of model agreement, we highlight that the areas of agreement are qualitatively similar to those studies. In a volcanic context, regions where extreme rainfall is projected to increase account for large portions of each of the continental volcanic arcs (the Cascades, the Alaskan Peninsula and Aleutian Range, Kamchatka, and Northern and Central Andes), parts of the Mediterranean and East African Rift system, and throughout the Sunda, Philippine, Ryuku, Japan, Kuril, Aleutian, and West Indies island arcs. Smaller subtropical island arcs, including the Bismarck Archipelago are also encompassed. On the other hand, models tend to agree that

extreme rainfall will decrease in parts of the Southern Andean Volcanic Zone and Rangitāhua (the Kermadec Islands), for example.

Of the 1234 Holocene-active subaerial volcanic systems included in the initial dataset, 716 (58 %) are situated in regions with a positive FMR (i.e., regions that are forecast to experience more extreme rainfall over the next 80 years) across the majority of GCMs (**Fig. 2b**). 244 of these (19 % of the initial dataset) have a mean (averaged over all models) FMR $\geq 5\%$ C⁻¹. Nineteen volcanoes (1.5 %) exhibit a mean FMR $\geq 20\%$ C⁻¹, all of which are located in the Galápagos, the East African Rift, and Papua New Guinea, between 3.125°S and 25.000°N. Highlighted in **Fig. 2b**, only 111 volcanoes (9 %) are located in regions anticipated to experience less extreme rainfall, with the remaining 407 (33 %) being associated with an ambiguous FMR (where fewer than 7 of the 9 models agreed with the sign of heavy precipitation change). We note that the proportion of volcanic systems associated with positive or negative FMR changes negligibly if the grid size is arbitrarily reduced. The aggregate FMR distribution of each of the models is approximately symmetrical around a median of 3.2 % C⁻¹, indicating that the majority of the globe is projected to experience an increase in extreme rainfall. When we consider only those grid cells containing active volcanic systems (**Fig. 2c**), we observe a lognormal distribution of volcanoes with positive FMR, with a mean value of $\sim 4.5\%$ C⁻¹ and a long tail on the positive side: the substantive majority of Earth's subaerial volcanic systems will be subject to more extreme rainfall with every increment of global warming over the remainder of the 21st century.

b. Models project an increase in heavy precipitation for most or all volcanic regions

The GVP subdivides Earth's volcanoes into 19 discrete regions, which are further subdivided into 101 subregions. Extracting areal averages of these volcanic regions (those grid cells containing at least one Holocene-active volcano: discrete coloured rectilinear polygons in **Fig. 3a**), we calculate the linear regression-based gradient of change in heavy precipitation versus global warming. A summary of the results is given in **Table 1**.

For each region, **Fig. 3b** indicates the distribution of models (out of a maximum of nine) that project a positive FMR: a concomitant increase in heavy rainfall with global warming. For the vast majority of volcanic regions (16/19: 84 %), most models project positive FMR. Of these, 13 (64 %) exhibit agreement across at least seven models, and for 8 regions (Antarctica; Atlantic Ocean; Alaska; Africa and Red Sea; México and Central America; Iceland and Arctic Ocean; West Indies; Canada and Western USA) all models forecast a positive FMR (42 % of all regions). There are zero volcanic regions for which at least seven of nine models project a negative FMR. This trend is echoed at the sub-regional scale (**Fig. 3b**): the majority of models forecast positive FMR for 74 of 101 subregions (73 %), and of these, 54 (53 %) exhibit agreement between at least seven models. There are no volcanic regions for which more than seven models project a negative FMR (cf. inset pie charts of **Fig. 3c**). At both the region and subregion scale, the observed distributions are statistically nonuniform, characterized by $\text{CDF}(\chi) \ll 0.01$. **Fig. 3c** shows the distribution of calculated gradients across models for each region. Note that majority-positive FMR distributions (e.g., Antarctica, Alaska, Atlantic Ocean, Mediterranean and Western Asia, Kamchatka and Mainland Asia: **Fig. 3c**) tend to be relatively tightly clustered, whereas for those regions where FMR is predominantly negative or ambiguous (e.g., Philippines, Kuril Islands, Hawai'i and Pacific Ocean: **Fig. 3c**), the distribution tends to be broader. The proportion of models exhibiting a positive FMR is indicated for each region by the marginal pie charts. We note that for eight regions, all models project a positive regional FMR (see also **Table 1**). Together, this emphasises the fact that when we observe reasonable inter-model concurrence in any given region, the result is usually that heavy rainfall is set to increase over the next 80 years.

Illustrative examples of regionally averaged climate projections are given in **Fig. 4a–f**, highlighted here due to the demonstrable risk of rainfall-induced hazard therein (data for all regions and subregions are provided in **Supplementary Information Figure S6**). The Atlantic ocean volcanic region (**Fig. 3a, Fig. 4a**) largely comprises island volcanoes characterised by a history of catastrophic collapse—including Tristan de Cunha, El Hierro, and Tenerife—a potential tsunamigenic hazard facilitated by wet climates [57]. The Canada and Western USA volcanic region (**Fig. 3a, Fig. 4b**) is predominantly composed of stratovolcanoes in the Cascade Range. The incidence of sector collapse at several Cascadian volcanoes (including Mount St Helens, Mt Adams, and Mt Baker) has been proposed to be triggered or exacerbated by historical climate change, including the attendant increase in humidity and rainfall [13]. Numerous volcanoes in the Cascade Range currently present a significant lahar threat to major population centres [58], with several exhibiting flank segments in excess of 20° slope pitch [56]. Notably, direct evidence of rainfall-triggered explosive activity has been reported for Mount St Helens [15]. The Alaska region (**Fig. 3a, Fig. 4c**)—including the Alaskan Peninsula, Aleutian Range, and Aleutian island arc—hosts volcanoes with the highest mean and partial flank inclines (in excess of 30 and 40°, respectively [56]). Holocene climate change has already been shown to have driven geologically recent volcanic sector collapse in parts of the Mediterranean and Western Asia region (**Fig. 3a, Fig. 4d**) [40], with these areas highlighted as becoming increasingly hazard-prone in the future [14]. The West Indies region (**Fig. 3a, Fig. 4e**) has similarly been highlighted [14], and hosts frequently active volcanoes such as Soufrière Hills where

primary volcanic activity is observably triggered by heavy rainfall [18,21]. Finally, Indonesia (**Fig. 3a, Fig. 4f**)—the world’s most volcanically active country and a volcanic region unto itself—is home to multiple volcanoes where explosive behaviour has been triggered by heavy rainfall. Notable examples are provided by excerpts from Smithsonian Institution’s Global Volcanism Program (GVP) Bulletin Reports:

“This first Bulletin report discussing Egon describes the sudden appearance of volcanic activity there in January 2004. Heavy rains fell over Egon and its surrounding area on 28 January ... followed at 1700 by an explosion and a black ash cloud rising ~ 750 m above the summit” [59];

“A sudden eruption at Karangetang on 6 August 2010 occurred without warning and caused considerable damage ... four people were confirmed dead and five were injured ... [An official noted] that the volcano erupted just after midnight when water from heavy rains had penetrated the volcano’s hot lava dome, causing the explosion.” [27];

“The phreatic eruption [of Lokon-Empung] was triggered by extensive rainfall; specifically, 602 mm of rain fell during January 2002 compared to 193 mm during December 2001. This excessive rainfall was thought to cause instability of the edifice.” [60];

“[O]n 22 February 2011, a phreatic eruption [of Lokon-Empung] ... was possibly triggered by high rainfall” [61].

Clearly, each of these volcanic regions appears particularly hazard-prone in terms of heavy rainfall-driven phenomena. Just as clearly, heavy rainfall is projected to increase in these regions by most or all climate models, thus heightening an already considerable threat to life, property, and infrastructure in the coming decades.

c. Climate change–induced hazards at individual volcanoes

Figure 4g–l presents the forced model responses at the scale of individual volcanic systems: Guagua Pichincha and Reventador, Ecuador; Soufrière Hills Volcano, Montserrat; Vesuvius, Italy; Gunung Merapi, Indonesia; and Fuego (Chi Q’aq’), Guatemala. These six volcanoes are chosen due to particularities of their eruptive histories, each of which illustrates the potential for increased hazard in the face of increased heavy precipitation. At Guagua Pichincha (**Fig. 3a, Fig. 4g**), cycles of explosivity have been anecdotally attributed to the timing of the rainy season [26]. A violent explosive eruption in 1993, triggered by “abnormally high” rainfall, resulted in the death of two volcanologists. Reventador (**Fig. 3a, Fig. 4h**), one of the most active volcanoes in Ecuador, is situated in a cloud-forest region already characterised by extremely heavy rainfall. Combined with its steep slopes [56], these factors contribute to the generation of frequent, often destructive, lahars. An analysis of Reventador’s historical eruption catalogue indicates a tendency towards erupting between December and May, when the volcano receives the majority of its annual rainfall. Soufrière Hills Volcano (**Fig. 3a, Fig. 4i**) is characterised by sensitivity to heavy rainfall: not only does lahar probability scale directly with rainfall intensity [62], but triggered primary volcanic activity has been reported frequently [18,20,21]. At Vesuvius (**Fig. 3a, Fig. 4j**), textural, geochemical, and anecdotal evidence of external water—possibly of meteoric origin—exists for several previous large eruptions [63,64]. As with Reventador, we note a tendency for large historic eruptions to occur between July and December. In 1998, a protracted period of extreme rainfall mobilised pyroclastic debris from Vesuvius and the Campi Flegrei systems and generated devastating debris flows, resulting in 160 fatalities with many more injured or displaced [65]. A statistical correlation between intense rainfall and explosive dome collapse has been reported at Gunung Merapi [16] (**Fig. 3a, Fig. 4k**). The risk of lahars at Merapi—invariably driven by rainfall [52]—is substantial, with lahar deposits covering an area of almost 300 km² in the region. Rainfall-triggered lahars at Merapi have been responsible for many deaths and the destruction of thousands of homes. The 2010–2011 rainy season at Merapi was not only associated with a cumulative rainfall amount more than 5 m greater than any year in the preceding decade (fostered by a strong La Niña period), but also a substantially higher lahar frequency than following previous eruptive events (as many as 59 in a single month [66]). Finally, at Fuego (**Fig. 3a, Fig. 4l**), heavy rainfall has been related to a host of eruptive and non-eruptive hazards, triggering plume emissions, seismic activity, and tilt changes [67], as well being directly related to frequently triggered lahars. With climate models almost exclusively projecting an increase in heavy precipitation with continued warming for each of these systems, it is highly probable that the already substantial risk to people, property, and infrastructure at these systems will be further amplified in the coming decades.

d. Lower Representative Concentration Pathway scenarios

RCP 8.5 is a greenhouse gas concentration trajectory associated with high and continuing emissions. For completeness, the analyses outlined above (**Methods**) were also repeated using lower concentration pathways: RCP 4.5 and RCP 2.6. Results from individual and compiled model analysis for RCP 4.5 are provided in **Supplementary Information Figure S2–3**, and those from individual and compiled model analysis for RCP 2.6

are provided in **Supplementary Information Figure S4–5**. RCP 4.5 is an intermediate scenario whereby emissions peak around 2040 before declining in the latter half of the century. This additional complexity results in globally lower agreement between models: we retrieve an agreement in the sign of FMR across 60.46 % of the globe (compared to 73.45 % for RCP 8.5). In turn, this means that it is not possible to obtain a robust estimate of the sign of FMR (i.e. agreement across seven or more models) for most (52 %) of the volcano catalogue used. However, it is evident that the proportion of volcanoes located in areas forecast to experience more extreme rainfall using the RCP 4.5 scenario remains significantly higher than volcanoes expected to experience less extreme rainfall: 506 volcanoes (42 % of the subaerial catalogue) versus 81 (7 %), respectively—a factor of six greater. RCP 2.6 is a “very stringent” pathway, which requires that global carbon dioxide emissions decrease to zero by 2100. Only seven of the climate models examined here (**Supplementary Information Table S1**) are available for RCP 2.6; accordingly, we define the threshold for inter-model agreement as 5/7 (i.e., 71.43 %: note that this is lower than that for RCP 8.5 and RCP 4.5, and that the results are not directly comparable). In this case, only 46.20 % of the globe meets this criterion, with the result that 64 % of the volcano inventory is not associated with a clear positive or negative FMR. Nevertheless, 34 % of the subaerial volcano catalogue is associated with increasing extreme rainfall under this scenario, compared to only 2 % associated with less: a factor of sixteen higher. In addition, there is broad qualitative agreement in the geographical distribution of positive and negative forced model response, both between CMIP5 models for each RCP (**Supplementary Information Figure S1, S2, S4**) and between the RCP 8.5, RCP 4.5, and RCP 2.6 datasets (**Figure 2, Supplementary Information Figure S3, S5**).

These additional analyses highlight that increasingly extreme rainfall in volcanic environments should be anticipated as the norm rather than the exception over the coming century—irrespective of the particular climate future modelled. The increased inter-model discrepancies coincident with decreasing RCP scenarios illustrate the inherent complexity in determining warming-driven geologic hazards; in particular, the potential for large multi-model ranges in projected outcomes is an inherent challenge in the intercomparison of an *ad hoc* ensemble of models [55]. Nevertheless, the proportion of volcanic systems projected to experience more extreme rainfall relative to the 2006 baseline is consistently greater than those for which extreme rainfall is projected to decrease, even under ambitious climate change mitigation strategies.

5. Conclusions and perspectives

In summary, we find that the majority of Holocene-active subaerial volcanic systems (716 volcanoes: 58 %) are confidently projected to experience more extreme rainfall as global temperatures continue to rise. Moreover, in some volcanic areas, heavy precipitation is projected to increase by as much as 46 % relative to the 2006 value for every degree of warming experienced over the next 80 years, based on a high emissions climate future. For another 33 % of volcanoes globally (in particular at mid-latitudes), there is not sufficient inter-model consensus to confidently estimate whether rainfall will become more or less extreme in the future. Broadly, these results hold across multiple emissions scenarios, and ultimately point to significant attendant implications for rainfall-related hazards at most of Earth’s subaerial volcanic systems.

Multidecadal catalogues of reports of volcanic activity reveal that rainfall has historically triggered, facilitated, or worsened primary volcanic activity or secondary hazards at over 170 subaerial volcanoes; a strong reminder that the influence of the hydrological cycle in volcanic systems can be substantial (see also **Fig. 1**). This link emphasises the importance of considering rainfall in the development of hazard mitigation strategies [21,62,68], and also underscores the importance of developing novel instrumental monitoring systems [69,70]. The incorporation of meteorological data into volcano monitoring systems has seen some limited adoption [71]; nevertheless, meteorological data is far from being a standard monitoring tool. Moreover, these results highlight the need for more interdisciplinary volcanological training, as proposed by [72]: compound disasters necessitate an increased range of expertise to effectively mitigate and manage. A number of updated climate models—i.e. the Coupled Model Intercomparison Project phase 6 (CMIP6) generation of GCMs—yield even greater projected warming than the CMIP5 models, although observationally constrained CMIP6 results align more readily with their CMIP5 counterparts [73]. The latter point notwithstanding, high-end global warmings cannot be discounted; rather, they emphasise the need for urgent adaption strategies [74].

While much previous emphasis has been placed on the effect of climate change on tropical volcanoes [75], we note that an increase in heavy precipitation is projected to occur with warming in many polar and temperate volcanic regions as well, including the Aleutian Arc, Western USA and Canada, and Antarctica and the South Sandwich Islands, as well as arid regions such as north Africa (**Supplementary Information Figure S6**). In resolving cross-model agreement at regional and local scales relevant for volcanic hazard, we demonstrate an explicit, geographically widespread link between global warming scenarios and the potential for increased volcanic hazard. We have not accounted for the influence of global warming on the dynamics of eruption plumes [76], nor for the proposed orographic feedback between heated volcanic summits and precipitation [77] which may serve to further exacerbate the influence of rainfall in volcanic regions. Moreover, it is inevitable that the volcanic response to increasingly extreme rainfall patterns will be strongly dependent on tectonic setting as a key determinant of the nature of hazard exhibited at any given volcano: a level of complexity that is not addressed here in detail. While previous studies have linked rainfall to variations in eruptivity at basaltic shield volcanoes [23,78,79], the majority of quantitative evidence of rainfall-induced volcanic hazard comes from intermediate, dome- and lahar-forming systems such as Soufrière Hills Volcano [18,80,81], Gunung Merapi [16,66], or Unzendake [82]. Further targeted research of the role of extreme rainfall

in other settings (e.g., continental rift zones) may provide invaluable context as to the sensitivity of individual systems or volcanic regions. We highlight that broader feedback mechanisms have also been proposed, including climate change-induced perturbations in crustal stress caused by ice-sheet and glacier wastage (McGuire, 2010), changes to axial and spin-rate of the Earth and realignment of the geoid [8,83], and rising sea levels [84,85], each of which have the potential to trigger subaerial volcanism.

In focussing on extreme climate indices here, we do not quantify the absolute amount of precipitation within the hydrogeological system at a given time. There is therefore additional complexity involved in mechanisms which involve a threshold cumulative amount of rainfall to enter the system, or rely on pre-existing system criticality. Quantifying any climate change-induced increase in volcanic activity is nontrivial, and the geospheric response to global warming and an increase in heavy precipitation will certainly be geographically variable [75]. Nevertheless, we may look to Earth system responses to previous long- and short-term changes in climate (e.g., **Fig. 1a**) to provide some insight into the future [86] where a committed global warming of 1.5–2 °C by 2100 appears inevitable [87].

Acknowledgements

We thank the climate modelling groups listed in **Supplementary Information Table S1** for generating and making publicly available their model data. We also thank the attendant data distribution centres and the World Climate Research Programme's Working Group on Coupled modelling, which is responsible for CMIP5. We also thank the Smithsonian Institution for developing and maintaining the Global Volcanism Program, from which data are openly available. We thank Indonesia's Meteorology, Climatology and Geophysics Agency (Badan Meteorologi, Klimatologi, dan Geofisika: BMKG) for making rainfall data publicly available. We thank Sharanya Majumdar, Hannah Derbyshire, Fabian Wadsworth, and the WHWN writing group for invaluable discussions. "vik" and "roma" colourmaps were created by Fabio Crameri (<http://doi.org/10.5281/zenodo.1243862>).

Funding Statement

This work was supported by funding from the NASA's Interdisciplinary Research in Earth Science (IDS) program (grant number 80NSSC17K0028 P00003).

Data Availability

All necessary data and code required are provided in the following GitHub repository: https://github.com/jifarquharson/rainfall-in-volcanic-regions/tree/main/Projects/Climate_forcing. This includes links to relevant open access repositories from which data were accessed. Model output data have been obtained through Earth System Grid Federation servers, in particular the node hosted by the Lawrence Livermore National Laboratory (<https://esgf-node.llnl.gov/search/cmip5/>). Data generated in the present study are available at the following repository: TBC. Additional datasets supporting this article have been uploaded as part of the Supplementary Material.

Competing interests

We have no competing interests.

Authors' Contributions

Conceptualisation: JIF, FA; Methodology: JIF; Investigation: JIF; Visualisation: JIF; Supervision: FA; Writing—original draft: JIF; Writing—review & editing: JIF, FA.

References

- Brönnimann S *et al.* 2019 Last phase of the Little Ice Age forced by volcanic eruptions. *Nature Geoscience* **12**, 650–656. (doi:10.1038/s41561-019-0402-y)
- Robock A. 2000 Volcanic eruptions and climate. *Reviews of Geophysics* **38**, 191–219. (doi:https://doi.org/10.1029/1998RG000054)
- Hyde WT, Crowley TJ. 2000 Probability of Future Climatically Significant Volcanic Eruptions. *Journal of Climate* **13**, 1445–1450. (doi:10.1175/1520-0442(2000)013<1445:LOFCSV>2.0.CO;2)
- Bethke I, Outten S, Otterå OH, Hawkins E, Wagner S, Sigl M, Thorne P. 2017 Potential volcanic impacts on future climate variability. *Nature Climate Change* **7**, 799–805. (doi:10.1038/nclimate3394)
- Aubry TJ *et al.* 2022 Impact of climate change on volcanic processes: current understanding and future challenges. *Bull Volcanol* **84**, 58. (doi:10.1007/s00445-022-01562-8)
- Cooper CL, Swindles GT, Savov IP, Schmidt A, Bacon KL. 2018 Evaluating the relationship between climate change and volcanism. *Earth-Science Reviews* **177**, 238–247. (doi:10.1016/j.earscirev.2017.11.009)
- Liggins F, Betts RA, McGuire B. 2010 Projected future climate changes in the context of geological and geomorphological hazards. *Philosophical Transactions of the Royal Society A: Mathematical, Physical and Engineering Sciences* **368**, 2347–2367. (doi:10.1098/rsta.2010.0072)

8. Rampino MR, Self S, Fairbridge RW. 1979 Can Rapid Climatic Change Cause Volcanic Eruptions? *Science* **206**, 826–829. (doi:10.1126/science.206.442.0.826)
9. Rowell CR, Jellinek AM, Hajimirza S, Aubry TJ. 2022 External Surface Water Influence on Explosive Eruption Dynamics, With Implications for Stratospheric Sulfur Delivery and Volcano-Climate Feedback. *Front. Earth Sci.* **10**, 788294. (doi:10.3389/feart.2022.788294)
10. Albino F, Pinel V, Sigmundsson F. 2010 Influence of surface load variations on eruption likelihood: application to two Icelandic subglacial volcanoes, Grímsvötn and Katla. *Geophys J Int* **181**, 1510–1524. (doi:10.1111/j.1365-246X.2010.04603.x)
11. Swindles GT *et al.* 2017 Climatic control on Icelandic volcanic activity during the mid-Holocene. *Geology* **46**, 47–50. (doi:10.1130/G39633.1)
12. Bay RC, Bramall N, Price PB. 2004 Bipolar correlation of volcanism with millennial climate change. *Proceedings of the National Academy of Sciences* **101**, 6341–6345. (doi:10.1073/pnas.0400323101)
13. Capra L. 2006 Abrupt climatic changes as triggering mechanisms of massive volcanic collapses. *Journal of Volcanology and Geothermal Research* **155**, 329–333. (doi:10.1016/j.jvolgeores.2006.04.009)
14. McGuire B. 2010 Potential for a hazardous geospheric response to projected future climate changes. *Philosophical Transactions of the Royal Society A: Mathematical, Physical and Engineering Sciences* **368**, 2317–2345. (doi:10.1098/rsta.2010.0080)
15. Mastin LG. 1994 Explosive tephra emissions at Mount St. Helens, 1989–1991: The violent escape of magmatic gas following storms? *GSA Bulletin* **106**, 175–185. (doi:10.1130/0016-7606(1994)106<0175:ETEA MS>2.3.CO;2)
16. Voight B, Constantine EK, Siswoidjoyo S, Torley R. 2000 Historical eruptions of Merapi Volcano, Central Java, Indonesia, 1768–1998. *Journal of Volcanology and Geothermal Research* **100**, 69–138. (doi:10.1016/S0377-0273(00)00134-7)
17. McBirney AR. 1955 Thoughts on the eruption of the nicaraguan volcano las pilas. *Bull Volcanol* **17**, 113–117. (doi:10.1007/BF02596048)
18. Matthews AJ, Barclay J, Carn S, Thompson G, Alexander J, Herd R, Williams C. 2002 Rainfall-induced volcanic activity on Montserrat. *Geophysical Research Letters* **29**, 22-1-22-4. (doi:https://doi.org/10.1029/2002GL014863)
19. Matthews AJ, Barclay J. 2004 A thermodynamical model for rainfall-triggered volcanic dome collapse. *Geophysical Research Letters* **31**. (doi:https://doi.org/10.1029/2003GL019310)
20. Hicks PD, Matthews AJ, Cooker MJ. 2010 Triggering of a volcanic dome collapse by rainwater infiltration. *J. Geophys. Res.* **115**, B09212. (doi:10.1029/2009JB006831)
21. Barclay J, Johnstone JE, Matthews AJ. 2006 Meteorological monitoring of an active volcano: Implications for eruption prediction. *Journal of Volcanology and Geothermal Research* **150**, 339–358. (doi:10.1016/j.jvolgeores.2005.07.020)
22. Carn S, Watts RB, Thompson G, Norton GE. 2004 Anatomy of a lava dome collapse: the 20 March 2000 event at Soufrière Hills Volcano, Montserrat. *Journal of Volcanology and Geothermal Research* **131**, 241–264. (doi:10.1016/S0377-0273(03)00364-0)
23. Farquharson JI, Amelung F. 2020 Extreme rainfall triggered the 2018 rift eruption at Kīlauea Volcano. *Nature* **580**, 491–495. (doi:10.1038/s41586-020-2172-5)
24. Sahoo S, Tiwari DK, Panda D, Kundu B. 2021 Eruption cycles of Mount Etna triggered by seasonal climatic Rainfall. *Journal of Geodynamics*, 101896. (doi:10.1016/j.jog.2021.101896)
25. McKee CO, Wallace DA, Almond RA, Talai B. 1981 Fatal hydro-eruption of Karkar volcano in 1979: Development of a maar-like crater. *Cooke-Ravian Volume of Volcanological Papers, Geological Survey of Papua New Guinea* **10**, 63–84.
26. Global Volcanism Program. 1993 Report on Guagua Pichincha (Ecuador). *Bulletin of the Global Volcanism Network* **18**. (doi:10.5479/si.GVP.BGVN199302-352020)
27. Global Volcanism Program. 2011 Report on Karangetang [Api Siau] (Indonesia). *Bulletin of the Global Volcanism Network* **36**. (doi:10.5479/si.GVP.BGVN201102-267020)
28. Lagmay AMF, Bagtasa G, Crisologo IA, Racoma BAB, David CPC. 2015 Volcanoes magnify Metro Manila's southwest monsoon rains and lethal floods. *Frontiers in Earth Science* **2**. (doi:10.3389/feart.2014.00036)

29. Németh K, Kósik S. 2020 Review of Explosive Hydrovolcanism. *Geosciences* **10**, 44. (doi:10.3390/geosciences10020044)
30. Poulidis AP, Renfrew IA, Matthews AJ. 2016 Thermally Induced Convective Circulation and Precipitation over an Isolated Volcano. *Journal of the Atmospheric Sciences* **73**, 1667–1686. (doi:10.1175/JAS-D-14-0327.1)
31. Paguican EMR, Lagmay AMF, Rodolfo KS, Rodolfo RS, Tengonciang AMP, Lapus MR, Baliatan EG, Obille EC. 2009 Extreme rainfall-induced lahars and dike breaching, 30 November 2006, Mayon Volcano, Philippines. *Bull Volcano* **71**, 845–857. (doi:10.1007/s00445-009-0268-8)
32. Kataoka KS, Matsumoto T, Saito T, Kawashima K, Nagahashi Y, Iyobe T, Sasaki A, Suzuki K. 2018 Lahar characteristics as a function of triggering mechanism at a seasonally snow-clad volcano: contrasting lahars following the 2014 phreatic eruption of Ontake Volcano, Japan. *Earth Planets Space* **70**, 113. (doi:10.1186/s40623-018-0873-x)
33. Baumann V, Bonadonna C, Cuomo S, Moscariello M, Biass S, Pistolesi M, Gattuso A. 2019 Mapping the susceptibility of rain-triggered lahars at Vulcano island (Italy) combining field characterization, geotechnical analysis, and numerical modelling. *Natural Hazards and Earth System Sciences* **19**, 2421–2449. (doi:https://doi.org/10.5194/nhess-19-2421-2019)
34. Ayonghe SN, Ntasin EB, Samalang P, Suh CE. 2004 The June 27, 2001 landslide on volcanic cones in Limbe, Mount Cameroon, West Africa. *Journal of African Earth Sciences* **39**, 435–439. (doi:10.1016/j.jafrearsci.2004.07.022)
35. Marques R, Zêzere J, Trigo R, Gaspar J, Trigo I. 2008 Rainfall patterns and critical values associated with landslides in Povoação County (São Miguel Island, Azores): relationships with the North Atlantic Oscillation. *Hydrological Processes* **22**, 478–494. (doi:https://doi.org/10.1002/hyp.6879)
36. Towhata I, Goto S, Goto S, Akima T, Tanaka J, Uchimura T, Wang G, Yamaguchi H, Aoyama S. 2021 Mechanism and future risk of slope instability induced by extreme rainfall event in Izu Oshima Island, Japan. *Nat Hazards* **105**, 501–530. (doi:10.1007/s11069-020-04321-0)
37. Eichenberger J, Ferrari A, Laloui L. 2013 Early warning thresholds for partially saturated slopes in volcanic ashes. *Computers and Geotechnics* **49**, 79–89. (doi:10.1016/j.compgeo.2012.11.002)
38. Manconi A, Longpré M-A, Walter TR, Troll VR, Hansteen TH. 2009 The effects of flank collapses on volcano plumbing systems. *Geology* **37**, 1099–1102. (doi:10.1130/G30104A.1)
39. Capra L, Bernal JP, Carrasco-Núñez G, Roverato M. 2013 Climatic fluctuations as a significant contributing factor for volcanic collapses. Evidence from Mexico during the Late Pleistocene. *Global and Planetary Change* **100**, 194–203. (doi:10.1016/j.gloplacha.2012.10.017)
40. Deeming KR, McGuire B, Harrop P. 2010 Climate forcing of volcano lateral collapse: evidence from Mount Etna, Sicily. *Philosophical Transactions of the Royal Society A: Mathematical, Physical and Engineering Sciences* **368**, 2559–2577. (doi:10.1098/rsta.2010.0054)
41. Tormey D. 2010 Managing the effects of accelerated glacial melting on volcanic collapse and debris flows: Planchon–Peteroa Volcano, Southern Andes. *Global and Planetary Change* **74**, 82–90. (doi:10.1016/j.gloplacha.2010.08.003)
42. Tebaldi C, Hayhoe K, Arblaster JM, Meehl GA. 2006 Going to the Extremes. *Climatic Change* **79**, 185–211. (doi:10.1007/s10584-006-9051-4)
43. Min S-K, Zhang X, Zwiers FW, Hegerl GC. 2011 Human contribution to more-intense precipitation extremes. *Nature* **470**, 378–381. (doi:10.1038/nature09763)
44. Gu G, Adler RF. 2015 Spatial Patterns of Global Precipitation Change and Variability during 1901–2010. *Journal of Climate* **28**, 4431–4453. (doi:10.1175/JCLI-D-14-00201.1)
45. Collins M, AchutaRao K, Ashok K, Bhandari S, Mitra AK, Prakash S, Srivastava R, Turner A. 2013 Observational challenges in evaluating climate models. *Nature Climate Change* **3**, 940–941. (doi:10.1038/nclimate2012)
46. Fischer EM, Sedláček J, Hawkins E, Knutti R. 2014 Models agree on forced response pattern of precipitation and temperature extremes. *Geophysical Research Letters* **41**, 8554–8562. (doi:https://doi.org/10.1002/2014GL062018)
47. Pfahl S, O’Gorman PA, Fischer EM. 2017 Understanding the regional pattern of projected future changes in extreme precipitation. *Nature Climate Change* **7**, 423–427. (doi:10.1038/nclimate3287)

48. Hodel DA *et al.* 2008 An 85-ka record of climate change in lowland Central America. *Quaternary Science Reviews* **27**, 1152–1165. (doi:10.1016/j.quascirev.2008.02.008)
49. Asmerom Y, Polyak VJ, Burns SJ. 2010 Variable winter moisture in the southwestern United States linked to rapid glacial climate shifts. *Nature Geoscience* **3**, 114–117. (doi:10.1038/ngeo754)
50. Grootes PM, Stuiver M, White JWC, Johnsen S, Jouzel J. 1993 Comparison of oxygen isotope records from the GISP2 and GRIP Greenland ice cores. *Nature* **366**, 552–554. (doi:10.1038/366552a0)
51. Pierson, Thomas C. T, Daag AS, Delos Reyes PJ, Regalado MaTM, Solidum RU, Tubianosa BS. 1996 Flow and Deposition of Posteruption Hot Lahars on the East Side of Mount Pinatubo, July–October 1991. In *Fire and Mud: Eruptions and Lahars of Mount Pinatubo, Philippines*, Quezon City: Philippine Institute of Volcanology and Seismology.
52. Lavigne F, Thouret JC, Voight B, Suwa H, Sumaryono A. 2000 Lahars at Merapi volcano, Central Java: an overview. *Journal of Volcanology and Geothermal Research* **100**, 423–456. (doi:10.1016/S0377-0273(00)00150-5)
53. Global Volcanism Program. 2013 Volcanoes of the World, v. 4.9.1 (17 Sep 2020).
54. Taylor KE, Stouffer RJ, Meehl GA. 2012 An Overview of CMIP5 and the Experiment Design. *Bulletin of the American Meteorological Society* **93**, 485–498. (doi:10.1175/BAMS-D-11-00094.1)
55. Tebaldi C, Knutti R. 2007 The use of the multi-model ensemble in probabilistic climate projections. *Philosophical Transactions of the Royal Society A: Mathematical, Physical and Engineering Sciences* **365**, 2053–2075. (doi:10.1098/rsta.2007.2076)
56. Grosse P, Euillades PA, Euillades LD, van Wyk de Vries B. 2013 A global database of composite volcano morphometry. *Bull Volcanol* **76**, 784. (doi:10.1007/s00445-013-0784-4)
57. Hürlimann M, Ledesma A, Martí J. 1999 Conditions favouring catastrophic landslides on Tenerife (Canary Islands). *Terra Nova* **11**, 106–111. (doi:https://doi.org/10.1046/j.1365-3121.1999.00233.x)
58. Hickson C. 1994 Character of volcanism, volcanic hazards, and risk, northern end of the Cascade magmatic arc, British Columbia and Washington State. *Bulletin - Geological Survey of Canada* **481**, 231–250.
59. Global Volcanism Program. 2004 Report on Egon (Indonesia). *Bulletin of the Global Volcanism Network* **29**. (doi:10.5479/si.GVP.BGVN200403-264160)
60. Global Volcanism Program. 2002 Report on Lokon-Empung (Indonesia). *Bulletin of the Global Volcanism Network* **27**. (doi:10.5479/si.GVP.BGVN200202-266100)
61. Global Volcanism Program. 2011 Report on Lokon-Empung (Indonesia). *Bulletin of the Global Volcanism Network* **36**. (doi:10.5479/si.GVP.BGVN201106-266100)
62. Jones R, Manville V, Peakall J, Froude MJ, Odibert HM. 2017 Real-time prediction of rain-triggered lahars: incorporating seasonality and catchment recovery. *Nat. Hazards Earth Syst. Sci.* **17**, 2301–2312. (doi:10.5194/nhess-17-2301-2017)
63. Scandone R, Giacomelli L, Gasparini P. 1993 Mount Vesuvius: 2000 years of volcanological observations. *Journal of Volcanology and Geothermal Research* **58**, 5–25. (doi:10.1016/0377-0273(93)90099-D)
64. Rolandi G, Barrella AM, Borrelli A. 1993 The 1631 eruption of Vesuvius. *Journal of Volcanology and Geothermal Research* **58**, 183–201. (doi:10.1016/0377-0273(93)90107-3)
65. Brondi F, Salvatori L. 2003 The 5–6 May 1998 mudflows in Campania, Italy. In *Lessons learnt from landslide disasters in Europe* (ed J Hervás), pp. 5–16.
66. de Bélizal E *et al.* 2013 Rain-triggered lahars following the 2010 eruption of Merapi volcano, Indonesia: A major risk. *Journal of Volcanology and Geothermal Research* **261**, 330–347. (doi:10.1016/j.jvolgeores.2013.01.010)
67. Global Volcanism Program. 1987 Report on Fuego (Guatemala). *Scientific Event Alert Network Bulletin* **12**. (doi:10.5479/si.GVP.SEAN198707-342090)
68. Pierson TC, Wood NJ, Driedger CL. 2014 Reducing risk from lahar hazards: concepts, case studies, and roles for scientists. *J Appl. Volcanol.* **3**, 16. (doi:10.1186/s13617-014-0016-4)
69. Nagatani K *et al.* 2018 Micro-unmanned aerial vehicle-based volcano observation system for debris flow evacuation warning. *Journal of Field Robotics* **35**, 1222–1241. (doi:https://doi.org/10.1002/rob.21834)

70. Sanderson RW, Matoza RS, Haymon RM, Steidl JH, Hegarty P. 2018 Lahar detection using infrasound: Pilot experiment at Mount Adams, WA. *AGU Fall Meeting Abstracts* **13**.
71. Global Volcanism Program. 2011 Report on Kirishimayama (Japan). *Bulletin of the Global Volcanism Network* **36**. (doi:10.5479/si.GVP.BGVN.201107-282090)
72. Fink J, Ajibade I. 2022 Future impacts of climate-induced compound disasters on volcano hazard assessment. *Bull Volcanol* **84**, 42. (doi:10.1007/s00445-022-01542-y)
73. Tokarska KB, Stolpe MB, Sippel S, Fischer EM, Smith CJ, Lehner F, Knutti R. 2020 Past warming trend constrains future warming in CMIP6 models. *Science Advances* **6**, eaaz9549. (doi:10.1126/sciadv.aaz9549)
74. Forster PM, Maycock AC, McKenna CM, Smith CJ. 2020 Latest climate models confirm need for urgent mitigation. *Nat. Clim. Chang.* **10**, 7–10. (doi:10.1038/s41558-019-0660-0)
75. McGuire B. 2010 Climate forcing of geological and geomorphological hazards. *Philosophical Transactions of the Royal Society A: Mathematical, Physical and Engineering Sciences* **368**, 2311–2315. (doi:10.1098/rsta.2010.0077)
76. In press. Impact of global warming on the rise of volcanic plumes and implications for future volcanic aerosol forcing - Aubry - 2016 - Journal of Geophysical Research: Atmospheres - Wiley Online Library. See <https://agupubs.onlinelibrary.wiley.com/doi/full/10.1002/2016JD025405> (accessed on 25 January 2021).
77. Poulidis AP, Takemi T, Iguchi M, Renfrew IA. 2017 Orographic effects on the transport and deposition of volcanic ash: A case study of Mount Sakurajima, Japan. *Journal of Geophysical Research: Atmospheres* **122**, 9332–9350. (doi:https://doi.org/10.1002/2017JD026595)
78. Klein FW. 1984 Eruption forecasting at Kilauea Volcano, Hawaii. *Journal of Geophysical Research: Solid Earth* **89**, 3059–3073. (doi:https://doi.org/10.1029/JB089iB05p03059)
79. Violette S, Marsily GD, Carbonnel JP, Goblet P, Ledoux E, Tijani SM, Vouille G. 2001 Can rainfall trigger volcanic eruptions? A mechanical stress model of an active volcano: 'Piton de la Fournaise', Reunion Island. *Terra Nova* **13**, 18–24. (doi:https://doi.org/10.1046/j.1365-3121.2001.00297.x)
80. Matthews AJ, Barclay J, Johnstone JE. 2009 The fast response of volcano-seismic activity to intense precipitation: Triggering of primary volcanic activity by rainfall at Soufrière Hills Volcano, Montserrat. *Journal of Volcanology and Geothermal Research* **184**, 405–415. (doi:10.1016/j.jvolgeores.2009.05.010)
81. Taron J, Elsworth D, Thompson G, Voight B. 2007 Mechanisms for rainfall-concurrent lava dome collapses at Soufrière Hills Volcano, 2000–2002. *Journal of Volcanology and Geothermal Research* **160**, 195–209. (doi:10.1016/j.jvolgeores.2006.10.003)
82. Yamasato H, Kitagawa S, Komiya M. 1998 Effect of rainfall on dacitic lava dome collapse at Unzen volcano, Japan. *Papers in Meteorology and Geophysics* **48**, 73–78. (doi:10.2467/mripapers.48.73)
83. Anderson DL. 1974 Earthquakes and the Rotation of the Earth. *Science* **186**, 49–50. (doi:10.1126/science.186.4158.49)
84. McGuire WJ, Howarth RJ, Firth CR, Solow AR, Pullen AD, Saunders SJ, Stewart IS, Vita-Finzi C. 1997 Correlation between rate of sea-level change and frequency of explosive volcanism in the Mediterranean. *Nature* **389**, 473–476. (doi:10.1038/38998)
85. Satow C, Gudmundsson A, Gertisser R, Ramsey CB, Bazargan M, Pyle DM, Wulf S, Miles AJ, Hardiman M. 2021 Eruptive activity of the Santorini Volcano controlled by sea-level rise and fall. *Nat. Geosci.* **14**, 586–592. (doi:10.1038/s41561-021-00783-4)
86. Knight J, Harrison S. 2013 The impacts of climate change on terrestrial Earth surface systems. *Nature Climate Change* **3**, 24–29. (doi:10.1038/nclimate1660)
87. Zhou C, Zelinka MD, Dessler AE, Wang M. 2021 Greater committed warming after accounting for the pattern effect. *Nature Climate Change* **11**, 132–136. (doi:10.1038/s41558-020-00955-x)

Tables

Table 1

Region			FMR					
abbr.	name	<i>n</i>	mean	st. dev.	median	min	max	# +ve
Mel	Melanesia and Australia	66	-3.04	4.97	-0.98	-	1.16	3
Phi	Philippines and SE Asia	47	-3.02	7.58	-2.54	-	10.84	3
Kur	Kuril Islands	41	0.97	3.35	0.79	-3.57	7.78	6
Ind	Indonesia	125	1.68	2.72	2.92	-3.39	4.23	7
Mid	Middle East and Indian Ocean	41	0.49	1.93	0.50	-3.02	3.63	6
Jap	Japan, Taiwan, and Marianas	105	-0.08	1.28	-0.56	-2.28	2.24	3
New	New Zealand to Fiji	30	1.93	2.36	1.60	-1.73	6.18	7
Haw	Hawai'i and Pacific Ocean	6	4.56	8.18	1.18	-1.59	25.93	6
Sou	South America	182	1.67	1.45	1.48	-0.90	4.63	8
Kam	Kamchatka and Mainland Asia;	85	1.45	1.12	1.63	-0.54	3.03	8
Med	Mediterranean and Western Asia	38	3.09	1.87	2.90	-0.14	7.38	8
Afr	Africa and Red Sea	119	6.24	5.53	5.40	0.44	16.43	9
Wes	West Indies	15	5.01	2.85	5.12	0.61	10.94	9
Ice	Iceland and Arctic Ocean	27	6.55	2.36	6.81	0.69	9.48	9
Can	Canada and Western USA	64	5.16	2.92	6.06	0.87	9.21	9
Méx	México and Central America	109	5.72	3.11	5.58	0.99	12.02	9
Atl	Atlantic Ocean	23	2.78	1.72	2.27	1.23	7.44	9
Ala	Alaska	86	5.25	2.70	4.61	1.25	11.86	9
Ant	Antarctica	25	5.38	1.37	4.92	3.57	8.05	9

Figures

Figure 1

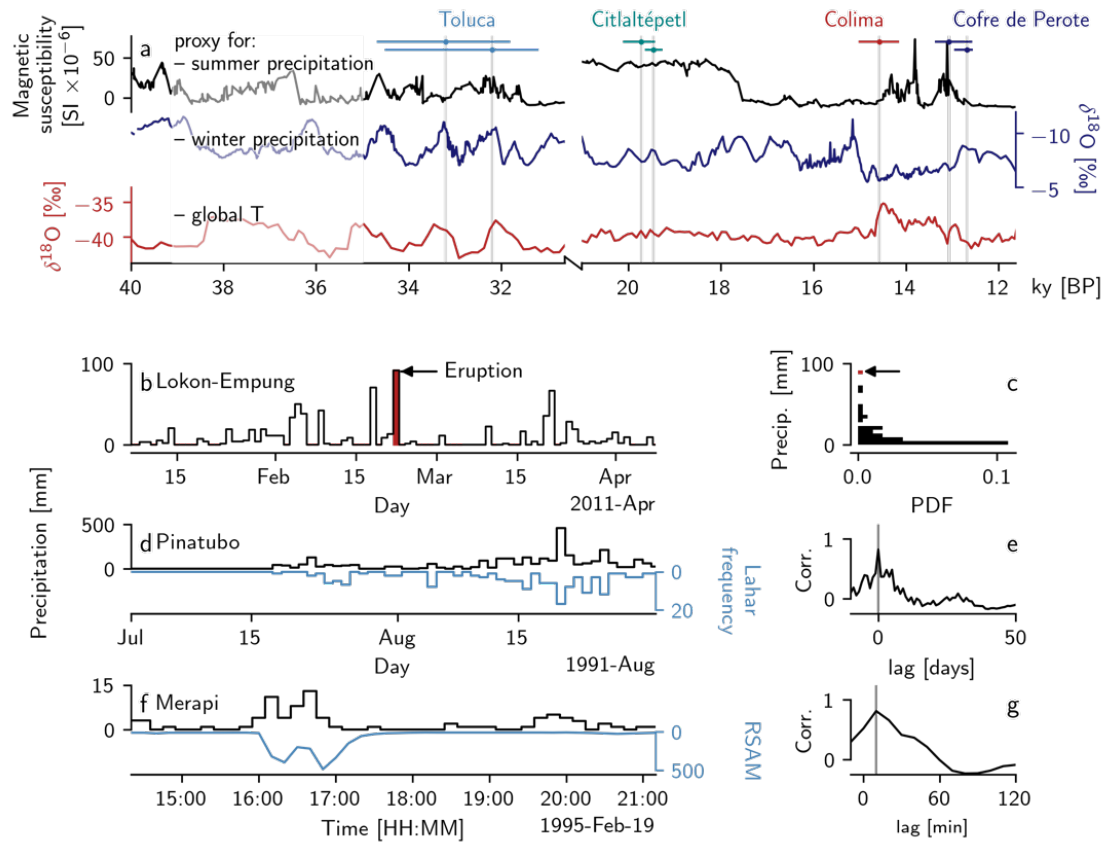


Figure 2

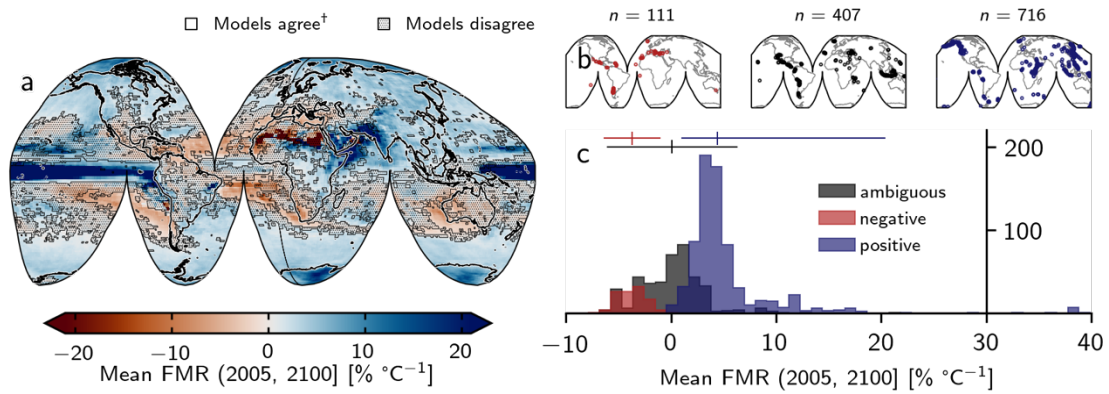


Figure 3

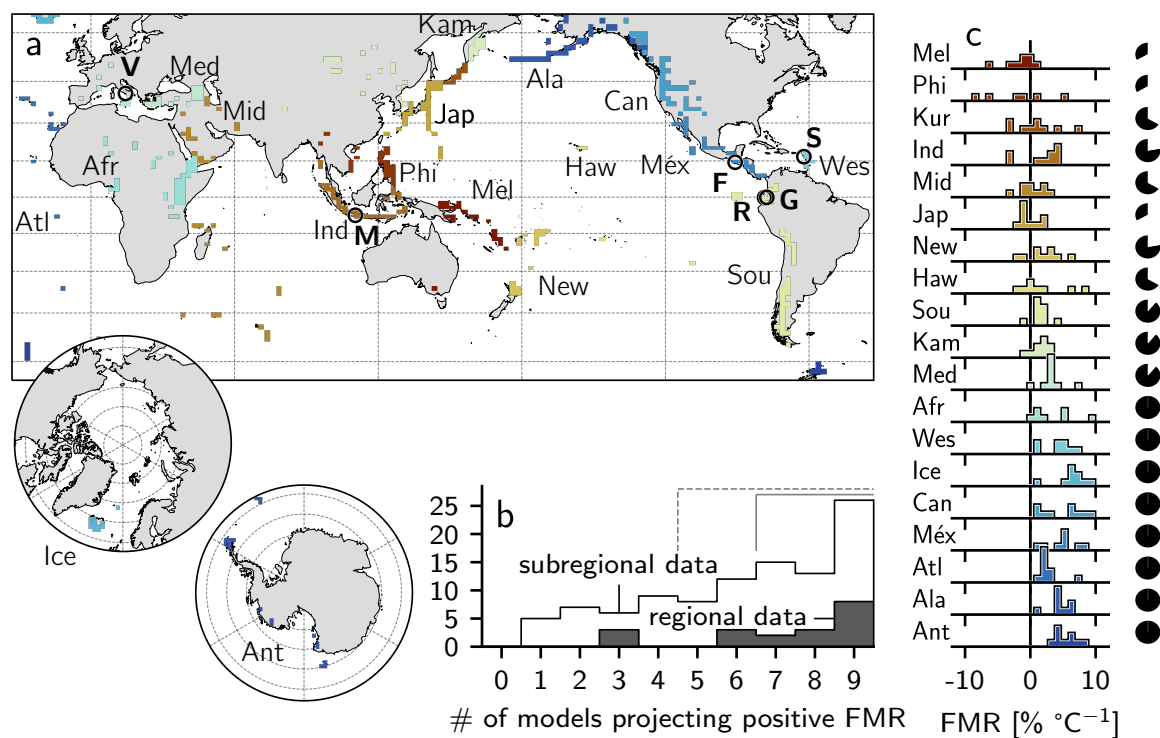


Figure 4

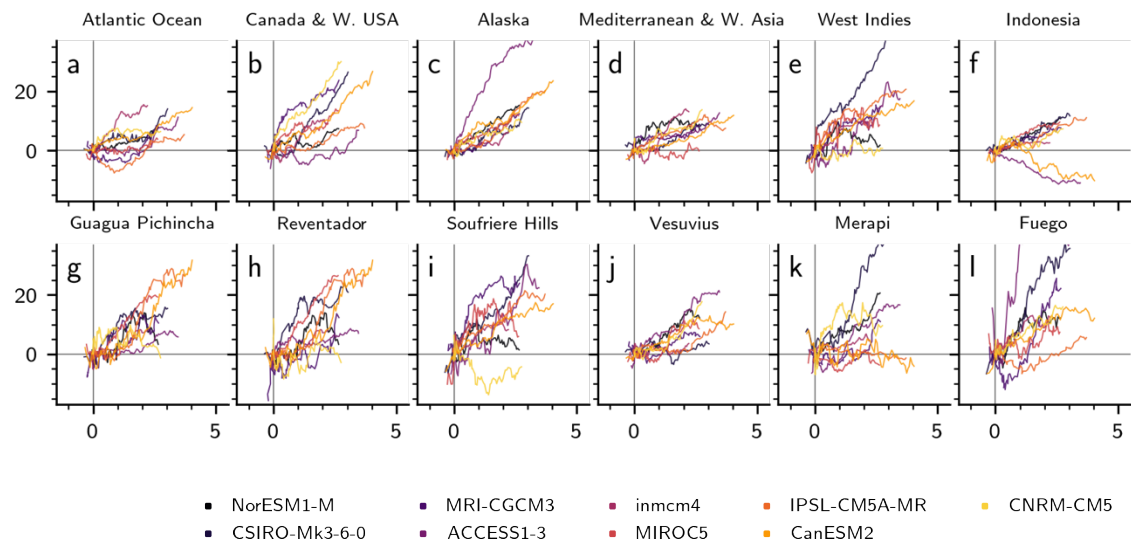


Figure 1. Extreme rainfall as a driver of volcanic hazards. **a** Pleistocene volcanic sector collapses of Volcán de Colima, Nevado de Toluca, Citlaltépetl, and Cofre de Perote (Mexico), reproduced after (Capra et al., 2013). Climate proxy data are described in the Methods. For each of the seven collapses, horizontal date ranges are indicated, as well as a vertical line highlighting the maximum probability collapse date. Note discontinuous x-axis. **b** The February 2011 eruption of Lokon-Empung is shown by a vertical line, alongside time-series of local precipitation data. **c** Lognormal distribution of precipitation data from **b**, with outlying value (corresponding to date of eruption) indicated. **d** Daily precipitation data (black) is plotted against the number of lahars per day (blue) observed at Pinatubo between July and September 1991. **e** Result of cross-correlation analysis of Pinatubo data shown in **d**, shown as correlation coefficient (“Corr.”) between daily precipitation and lahar frequency versus lag. **f** Precipitation in ten-minute bins at Merapi volcano, alongside the RSAM value at the same temporal resolution. RSAM maxima reflect peak lahar surges. **g** Result of cross-correlation analysis of Merapi data shown in **f**, shown as correlation coefficient between ten-minute precipitation and RSAM value versus lag. Refer to **Methods** for all data sources.

Figure 2. Breakdown of mean forced model response. **a** Global mean forced model response (FMR) calculated from all models. Shaded area indicates those regions where fewer than seven of nine models agreed on the sign of change (26.55 %). †at least seven of nine models agree on the sign of change. **b** Subaerial volcano geolocations separated according to whether models agree on a decrease in heavy precipitation with increased warming (red: “negative”; $n = 111$); the precipitation response is ambiguous due to lack of model agreement (black: “ambiguous”; $n = 407$); models agree on an increase in heavy precipitation with increased warming (blue: “positive”; $n = 716$). n indicates the number of discrete Holocene-active volcanic systems in each category. **c** Histogram of mean FMR for each group of volcanoes (as in **b**). Mean and two standard deviation range are indicated by the vertical and horizontal lines, respectively (**Methods**).

Figure 3. Regional and sub-regional spatial averages. **a** Map indicating the noncontiguous spatial extent over which regional data are averaged. Circle markers indicate individual volcanoes shown in Figure 4. V = Vesuvius, M = Merapi, F = Fuego, R = Reventador, G = Guagua Pichincha, S = Soufrière Hills Volcano. [Inset] polar regions. Regions are represented by discrete colored rectilinear polygons. Ant = Antarctica; Atl = Atlantic Ocean; Sou = South America; Ala = Alaska; Kur = Kuril Islands; Ind = Indonesia; Mid = Middle East and Indian Ocean; Phi = Philippines and SE Asia; Méx = México and Central America; Jap = Japan, Taiwan, and Marianas; Kam = Kamchatka and Mainland Asia; Med = Mediterranean and Western Asia; New = New Zealand to Fiji; Haw = Hawai’i and Pacific Ocean; Ice = Iceland and Arctic Ocean; Afr = Africa and Red Sea; Wes = West Indies; Mel = Melanesia and Australia; Can = Canada and Western USA. **b** Bar chart of the number of regions and subregions where x number of models project a spatially averaged forced model response (FMR) > 0 (i.e., a concomitant increase in heavy precipitation and global mean temperature). Dashed bracket indicates the majority of models, solid bracket indicates 7 or more out of 9 models. **c** Inter-model distributions of calculated FMR for each region. Marginal pie charts indicate the proportion of models that project a positive FMR per region (out of maximum of nine).

Figure 4. Forced model responses at different spatial scales. **a–f** Percent change in modeled heavy rainfall per degree of global warming. Data are shown as a 30-yr rolling mean, normalized to January 2021. Data are areal averages (see **Figure 3** for areal extent of each region). **g–l** As **a–f**, for individual volcanic systems. Data correspond to the bounding pixel for each model (see **Methods**). Volcano locations are shown in **Figure 3**.

Table 1. Model analysis results. Abbreviation corresponds to the three-letter code on **Figure 3**. n is the number of historically active volcanoes within the region. Mean and median FMR values are given, along with standard deviation from the mean. “min” and “max” refer to the minimum and maximum calculated values of FMR for each region. “# +ve” refers to the number of models (out of nine) that yield a positive FMR value (see **Figure 3c**).